List of Supplementary Information:

Supplementary Note 1: Mathematical model

Supplementary Note 2: Parameter estimation

Supplementary Note 3: Model non-dimensionalization

Supplementary Note 4: Additional figures

Supplementary Figure 1: Ang1 and Ang2 activation of Tie2 in a concentration-dependent manner. Reconstruction of the curve f_1 and f_2 from the data shown in Figs 1A and 1B in [1]. The figure is embedded in Supplementary Note S.1.

Supplementary Figure 2: Oxygen-dependent VEGF expression. Plot of the $h_{1,V}(O_2)$ function modeling the effect of oxygen concentration on VEGF expression. Red circles represent the experimental values taken from in [2]. The figure is embedded in Supplementary Note S.2.

Supplementary Figure 3: Sensitivity analysis on P/T ratio. Percentage variations $\mathbb{V}$ in the P/T (phosphorylated/total Tie2) ratio are reported for different values of m and b within a range $\pm 50\%$ with respect to their baseline estimations. The figure is embedded in Supplementary Note 2.

Supplementary Figure 4: Limit cycle. Phase diagrams of system (19) are presented for the parameter values specified in the Supplementary Table 2, focusing on the advanced-stage tumor scenario. These diagrams illustrate the emergence of a limit cycle within the oxygen-cell-cytokines feedback loop, corresponding to sustained cyclic hypoxia. Left plot: oxygen-endothelial cells diagram. Middle plot: oxygen-tumor cells diagram. Right plot: oxygen-cytokines diagram. The figure is embedded in Supplementary Note 4.

Supplementary Figure 5: Sustained (over time) slow-cyclic hypoxia in advanced-stage tumor. Qualitative results for oxygen, endothelial cells, tumor cells, and cytokines obtained from the evolution of system (19) for parameter values listed in the Supplementary Table 2 are shown for the advanced-stage tumor case. The red and blue dashed line in the oxygen plot refers to normoxia-hypoxia (5% O_2) and hypoxia-severe hypoxia (1% O_2) thresholds, respectively. Simulations are run for 180 days to show how cyclic hypoxia is sustained over time. All the y-axis refer to non-dimensionalized densities or concentrations of the indicated agents. The figure is embedded in Supplementary Note 4.

Supplementary Figure 6: Early-stage tumor evolution. Qualitative results of the evolution of the system (19) for parameter values listed in the Supplementary Table 2 in the early-stage tumor scenario for $t \in [0, T_0]$ and $T_0 = 0.27$ days. (A) shows the qualitative relationship between Y and the equilibrium state of the dimerized form of VEGFR (x^*), i.e., x^* as a function of $Y := \frac{k_{\text{on}}}{k_{\text{off}}} V$, where k_{on} and k_{off} are the binding and unbinding rates between V and u, respectively [3]. The blue marker indicates the value of x^* for $V(0)$, while the green marker indicates the value of x^* at $V_{\max}$, which represents a numerically observed upper bound for the ligand concentration. Red dashed lines in (A) and (B) refer to the threshold th_x, above which EC proliferation is stimulated, the one in (E) plot to the threshold th_{pTie2}, below which vessel destabilization might happen, the red and blue in (F) refers to normoxia-hypoxia (5% O_2) and hypoxia-severe hypoxia (1% O_2) thresholds, respectively. All the y-axis refer to non-dimensionalized density or concentrations. The figure is embedded in Supplementary Note 4.

Supplementary Figure 7: Advanced-stage tumor evolution. Qualitative results of the evolution of the system (19) for parameter values listed in the Supplementary Table 2 in the advance-stage tumor scenario for $t \in [0, T_0]$ and $T_0 = 0.27$ days. (A) shows the qualitative relationship between Y and the equilibrium state of the dimerized form of VEGFR (x^*), i.e., x^* as a function of $Y := \frac{k_{\text{on}}}{k_{\text{off}}} V$, where k_{on} and k_{off} are the binding and unbinding rates between V and u, respectively [3]. The blue marker indicates the value of x^* for $V(0)$, while the green marker indicates the value of x^* at $V_{\max}$, which represents a numerically observed upper bound for the ligand concentration. Red dashed lines in (A) and (B) refer to the threshold th_x, above which EC proliferation is stimulated, the one in (E) plot to the threshold th_{pTie2}, below which vessel destabilization might happen, the red and blue in (F) refers to normoxia-hypoxia (5% O_2) and hypoxia-severe hypoxia (1% O_2) thresholds, respectively. All the y-axis refer to non-dimensionalized density or concentrations. The figure is embedded in Supplementary Note 4.

Supplementary Table 1. Independent variables of system (19), their meaning, and their corresponding units of measure. The table is embedded in Supplementary Note S.4.

Supplementary Table 2. Estimation of the model parameters involved in system (19). (*) indicates that the corresponding parameter value has been estimated from the data provided in this work or adapted from ranges reported in the literature, as detailed explained in Supplementary Note 2. The table is embedded in Supplementary Note 2.

Supplementary Table 3. Maximum percentage variations in the evolution of tumor cells C and oxygen O_2 in the early-stage tumor scenario are reported when varying the value of $\theta \in \{m, b, d_C, k_{Cyt}, d_{Cyt}\}$. Precisely, $\underline{\theta} := \theta_B - \theta_B/2$ and $\widehat{\theta} := \theta_B + \theta_B/2$ represent the minimum and maximum parameter values used in the analysis. The table is embedded in Supplementary Note 2.

Supplementary Table 4. Maximum percentage variations obtained in the evolution of tumor cells C and oxygen O_2 in the advanced-stage tumor scenario when varying the value of $\theta \in \{m, b\}$. Precisely, $\underline{\theta} := \theta_B - \theta_B/2$ and $\widehat{\theta} := \theta_B + \theta_B/2$ represent the minimum and maximum parameter values used in the analysis. The table is embedded in Supplementary Note 2.

Supplementary Table 5. Reference values for the different agents involved in system (19). (*) indicates that the corresponding parameter value has been estimated from the data provided in this work or adapted from ranges reported in the literature, as detailed explained in Supplementary Note 2. The table is embedded in Supplementary Note 3.

Supplementary References

Supplementary Note 1: Mathematical model

We propose a novel mathematical model that characterizes the interactions between cellular and molecular components involved in the tumor angiogenic process. In particular, we examine three compartments (or modules), with a specific focus on the cellular module that comprises two distinct cell populations - tumor cells and endothelial cells (ECs) - interacting in response to variations in oxygen and cytokine concentrations. We further include two modules that account for the Tie-Ang and the VEGF-VEGFR signaling pathways. Figure (1) in the main text illustrates the model, its compartments, and the interactions between them.

S.1 Angiopoietin module

The Tie-Ang signaling system involves two types of angiopoietin ligands: Ang1 and Ang2. Both ligands bind to the Tie2 receptor. This receptor has two states: an inactive one and its phosphorylated form, pTie2, which is responsible for activating the signaling downstream of the active Tie receptor. In the Ang1/Tie2 system, the ligand is tetravalent and the receptor is monovalent, meaning that one Ang1 molecule binds to four Tie2 receptors, while each Tie2 can bind to a single Ang1 molecule. Four Tie2 receptors and one Ang1 molecule form the complex (Ang1(Tie2)4). Conversely, in the Ang2/Tie2 system, the ligand is bivalent (see Assumption 1 for further details), meaning that one Ang2 molecule binds to two Tie2 receptors, while each Tie2 can bind to a single Ang2 molecule. Two Tie2 receptors and one Ang2 molecule form the complex (Ang2(Tie2)2). The formation of these complexes, in a dose-dependent manner, allows for the phosphorylation of the receptor. Precisely, the angiopoietin module takes the following variables into account.

- The Ang1 ligand exists in oligomeric form and interacts with the Tie2 receptor. Specifically, the tetrameric configuration of Ang1 binds to Tie2, leading to the clustering of the receptor into a tetrameric structure and to its activation [4, 5, 6].
- (Ang1(Tie2)4) is the tetrameric form of the Ang1-Tie2 complex.
- The Ang2 ligand is considered an antagonist to Ang1, as both Ang1 and Ang2 compete for the same binding site on the Tie2 receptor [7, 8, 1]. Native Ang2 is primarily found in a dimeric form (75%, with 16% in trimeric form and 9% in tetrameric form). Consequently, the prevalence of low oligomeric forms of Ang2, in comparison to Ang1, restricts the ability of Ang2 to activate Tie2 [9].
- (Ang2(Tie2)2) is the dimeric form of the Ang2-Tie2 complex.
- The Tie2 receptor is expressed on the membrane of endothelial cells, and it can bind to both Ang1 and Ang2.
- pTie2 refers to the phosphorylated form of Tie2, and it plays a crucial role in Tie2 signaling.

Their evolution is governed by the following system of ordinary differential equations (ODEs):

$$\begin{cases} \dfrac{d\,\mathrm{Ang1}}{dt} = -F_1 \\ \dfrac{d\,(\mathrm{Ang1(Tie2)4})}{dt} = F_1 \\ \dfrac{d\,\mathrm{Ang2}}{dt} = -F_2 + h_{\mathrm{Ang2}}(V)E - d_{\mathrm{Ang2}}\,\mathrm{Ang2} \\ \dfrac{d\,(\mathrm{Ang2(Tie2)2})}{dt} = F_2 \\ \dfrac{d\,\mathrm{Tie2}}{dt} = -4F_1 - 2F_2\,. \end{cases} \tag{1}$$

The rates F_1 and F_2 are given by:

$$F_1 = k_1\,\mathrm{Ang1}\,\mathrm{Tie2}^4 - k_{-1}\,(\mathrm{Ang1(Tie2)4}) \tag{2}$$

$$F_2 = k_2\,\mathrm{Ang2}\,\mathrm{Tie2}^2 - k_{-2}\,(\mathrm{Ang2(Tie2)2}) \tag{3}$$

where k_1 and k_2 are the association constants of Ang1-Tie2 and Ang2-Tie2, and k_{-1} and k_{-2} are the dissociation constants. Ang2 is assumed to decay at a rate d_{Ang2}. The function $h_{\mathrm{Ang2}}(V)E$ describes the production of Ang2

by ECs (E) under VEGF (V) stimulation. For this function, we consider a model that allows for a saturation effect at high concentrations of VEGF:

$$h_{\text{Ang2}}(V) := k_{\text{Ang2}} V \tanh(V)$$

where the constant k_{Ang2} is the Ang2 production rate. Various studies have investigated the impact of VEGF and endothelial cells on the expression of Ang2. In [10], the authors observed that VEGF alone induces an increase in both Ang2 mRNA expression and transcription in a time- and concentration-dependent manner, without affecting its half-life. Additionally, [11, 12] have demonstrated cell type-specific regulation of Ang2 in response to hypoxia and HIF activation. In both bovine [11] and human [13] microvascular endothelial cells, both hypoxia and VEGF induced Ang2 expression. However, note that, while VEGF is necessary, it is not sufficient for angiogenesis to occur.

The system (1) is coupled with the model for pTie2 dynamics. For its formulation, we consider some experimental results described in [7, 1]. Specifically, in [7], endothelial cells (HUVECs) were stimulated with Ang1 both in the absence and presence of Ang2. Phosphorylated (P) and total (T) Tie2 levels were measured, and the P/T ratio values (means ± standard deviations) were reported in Figure 6B of [7]. These results demonstrated a certain degree of antagonism between the two ligands, Ang1 and Ang2, in their effect on Tie2 activation. Independently, both ligands induce Tie2 activation in a dose-dependent manner. However, when combined, a non-linear relationship between their concentrations and Tie2 phosphorylation is observed. Specifically, at low concentrations, Ang2 cooperates with Ang1 to promote Tie2 phosphorylation, whereas, at high concentrations, Ang2 and Ang1 antagonize each other, thereby inhibiting pTie2. In [1], phosphorylation of Tie2 was analyzed by stimulating HUVECs with Ang1 and Ang2 separately. The results, provided in Figure 1A and 1B of [1], showed how Ang1 and Ang2 activate Tie2 in a concentration-dependent manner, however Tie2 phosphorylation induced by Ang1 is considerably higher compared with Ang2. Similar results on the stimulation of Tie2 phosphorylation by Ang1 have also been reported in [14, 15]. To capture these behaviors of pTie2 upon stimulation with Ang1 and Ang2, we consider the data derived from Figures 6B in [7] and 1A-B in [1]. We start from [1], where the percentage of pTie2 is plotted against the initial concentrations of Ang1 and Ang2. Let $A_{1,0}$ and $A_{2,0}$ denote the initial concentration of Ang1 (Ang1 at $t = 0$) and Ang2 (Ang2 at $t = 0$), respectively. From Figures 1A and 1B, we can reconstruct the functions as follows:

$$f_1 : (A_{1,0}, 0) \to \text{pTie2}$$

$$f_2 : (0, A_{2,0}) \to \text{pTie2}\,.$$

These functions describe the levels of pTie2 in relation to the initial concentrations of Ang1 and Ang2. We directly take the pTie2 values from [1] for the different ligand concentrations that were experimentally tested. Using these values, we interpolate to define the curves, as shown in the Supplementary Figure 1. As we have

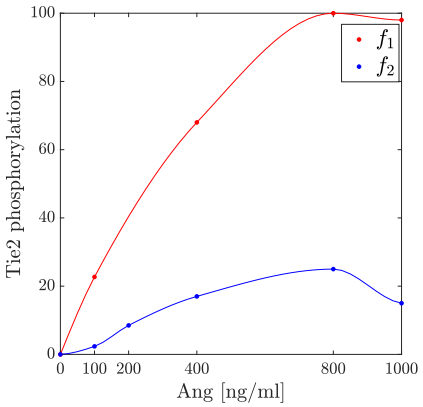

Supplementary Figure 1: **Ang1 and Ang2 activation of Tie2 in a concentration-dependent manner.** Reconstruction of the curve f_1 and f_2 from the data shown in Figs 1A and 1B in [1].

found no available experimental data concerning quantitative studies on the combined effect of Ang1 and Ang2 on pTie2, we define the following function $\tilde{f}$ based on the previously constructed functions f_1 and f_2:

$$\tilde{f} : (A_{1,0}, A_{2,0}) \to \text{pTie2}\,.$$

It estimates pTie2 levels for mixed combinations of Ang1 and Ang2 initial concentrations. Assuming $A_{1,0}, A_{2,0} \neq 0$ and defining the weights $d_1 = 1/A_{2,0}$ and $d_2 = 1/A_{1,0}$, $\tilde{f}$ can be described as a weighted sum of f_1 and f_2:

$$\tilde{f} = \frac{1}{d_1 + d_2} \left(d_1 f_1 + d_2 f_2\right)\,.$$

By defining the quantities

$$r_1 = \frac{d_1}{d_1 + d_2} = \frac{A_{1,0}}{A_{1,0} + A_{2,0}} \quad \text{and} \quad r_2 = \frac{d_2}{d_1 + d_2} = \frac{A_{2,0}}{A_{1,0} + A_{2,0}},$$

$\tilde{f}$ can be rewritten as

$$\tilde{f} = r_1 f_1 + r_2 f_2 , \tag{4}$$

Thus, for $A_{1,0} = 0$ (respectively $A_{2,0} = 0$), $\tilde{f}$ is identical to f_2 (respectively f_1). Conversely, the higher the value of $A_{j,0}$, the smaller the impact of f_i on $\tilde{f}$, for $i \neq j$. This relationship ensures that the contribution of each ligand's initial concentration is appropriately weighted, reflecting the observed antagonistic and cooperative interactions between Ang1 and Ang2 on pTie2 activation. To describe the equation for the evolution of the P/T ratio $R = \text{pTie2}/\,\text{Tie2}$, we consider the data provided in Figure 6B in [7], where the P/T ratio is analyzed for a fixed initial concentration of Ang1 and increasing initial concentrations of Ang2. Thus, we start by deriving the equation for the evolution of R with respect to $A_{1,0}$ and $A_{2,0}$. Specifically, given $f = \tilde{f}/\,\text{Tie2}$, we set

$$\sum_{i=1}^{2} \frac{1}{r_i} \frac{dR}{d\,A_{i,0}} = F(R) . \tag{5}$$

This can be rewritten as

$$\begin{aligned} \sum_{i=1}^{2} \frac{1}{r_i} \frac{dR}{d\,A_{i,0}} = F(R) &\iff \sum_{i=1}^{2} \frac{1}{r_i} \frac{dR}{df} \frac{df}{d\,A_{i,0}} = F(R) \\ &\iff \sum_{i=1}^{2} \frac{1}{r_i} \frac{dR}{dt} \frac{dt}{df} \frac{df}{d\,A_{i,0}} = F(R) \\ &\iff \frac{dR}{dt} = F(R) \frac{1}{\sum_{i=1}^{2} \frac{1}{r_i} \frac{df}{d\,A_{i,0}}} \frac{df}{dt} , \end{aligned} \tag{6}$$

where

$$\frac{df}{dt} = \frac{d}{dt}\left(\frac{\tilde{f}}{\text{Tie2}}\right) = -\frac{\tilde{f}}{\text{Tie2}^2} \frac{d\,\text{Tie2}}{dt} . \tag{7}$$

The derived equation for the temporal evolution of R allows to take into account both the evolution of the levels of R with respect to $A_{1,0}$ and $A_{2,0}$ and the evolution of the receptor Tie2, thus the evolution of the entire signaling route connected to it. To derive the expression of $\frac{df}{d\,A_{i,0}}$, from system (1), we first obtain

$$\begin{cases} \dfrac{d(\text{Ang1(Tie2)4})}{d\,A_{i,0}} = k_1 \displaystyle\int_0^t e^{k_{-1}(s-t)} \left(4\,\text{Tie2}^3\,\text{Ang1} \frac{d\,\text{Tie2}}{d\,A_{i,0}} + \text{Tie2}^4 \frac{d\,\text{Ang1}}{d\,A_{i,0}} \right) ds \\ \dfrac{d(\text{Ang2(Tie2)2})}{d\,A_{i,0}} = k_2 \displaystyle\int_0^t e^{k_{-2}(s-t)} \left(2\,\text{Tie2}\,\text{Ang2} \frac{d\,\text{Tie2}}{d\,A_{i,0}} + \text{Tie2}^2 \frac{d\text{Ang2}}{d\,A_{i,0}} \right) ds \end{cases}$$

for $i = 1, 2$. Then, we calculate the expressions for $y_{i,j} = \frac{d\text{Ang}i}{d\,A_{j,0}}$ and $z_i = \frac{d\,\text{Tie2}}{d\,A_{i,0}}$, for $i, j = 1, 2$:

$$\begin{cases} \dfrac{dy_{1,j}}{dt} = -k_1 y_{1,j}\,\text{Tie2}^4 - 4k_1\,\text{Tie2}^3\,\text{Ang1}\,z_j + k_1 k_{-1} \displaystyle\int_0^t e^{k_{-1}(s-t)} \left(4\,\text{Tie2}^3\,\text{Ang1}\,z_j + \text{Tie2}^4 y_{1,j}\right) ds \\ \dfrac{dy_{2,j}}{dt} = -k_2 y_{2,j}\,\text{Tie2}^2 - 2k_2\,\text{Tie2}\,\text{Ang2}\,z_j + k_2 k_{-2} \displaystyle\int_0^t e^{k_{-2}(s-t)} \left(2\,\text{Tie2}\,\text{Ang2}\,z_j + \text{Tie2}^2 y_{2,j}\right) ds \\ \dfrac{dz_i}{dt} = \dfrac{dy_{1,i}}{dt} + \dfrac{dy_{2,i}}{dt} . \end{cases}$$

Recalling the expression of $\tilde{f}$ given in (4) and $f = \tilde{f}/\text{Tie2}$, and defining $\tilde{r}_j := r_j/(A_{1,0} + A_{2,0})$, we derive

$$\frac{df}{d\,A_{i,0}} = \frac{1}{\text{Tie2}} \left((-1)^{i+1} \tilde{r}_j (f_1 - f_2) + r_i \frac{df_i}{d\,A_{i,0}} - z_i f \right)$$

for $i, j = 1, 2$, $j \neq i$. This allows us to derive the following expression

$$\sum_{i=1}^{2} \frac{1}{r_i} \frac{df}{d[A_{i,0}]} = \frac{1}{\text{Tie2}} \sum_{i=1}^{2} \left(d_i r_i (-1)^{i+1} (f_2 - f_1) - \frac{1}{r_i} z_i f + \frac{d f_i}{d A_{i,0}} \right) . \tag{8}$$

Thus, plugging (8) and (7) into (6), we get

$$\frac{d R}{dt} = - \frac{F(R)}{\sum_{i=1}^{2} \left(d_i r_i (-1)^{i+1} (f_2 - f_1) - \frac{1}{r_i} z_i f + \frac{d f_i}{d A_{i,0}} \right)} f \, \frac{d \, \text{Tie2}}{dt} . \tag{9}$$

From (9), using the definition of R, we derive

$$\frac{d\text{pTie2}}{dt} = \frac{d \, \text{Tie2}}{dt} \left[R - \frac{F(R)}{\sum_{i=1}^{2} \left(d_i r_i (-1)^{i+1} (f_2 - f_1) - \frac{1}{r_i} z_i f + \frac{d f_i}{d A_{i,0}} \right)} \tilde{f} \right] := \frac{d \, \text{Tie2}}{dt} P(R) . \tag{10}$$

We define the function F to account for two main mechanisms. Precisely, F can be described as

$$F = G(\text{Ang1}, \text{Ang2}, \text{Tie2}) R \, N(R) - d_R R \tag{11}$$

where the last term models a natural decay at rate d_R, while $G(\text{Ang1}, \text{Ang2}, \text{Tie2})$ and $N(R)$ are the BEWARE operator [16] and the growth rate function for R, respectively. BEWARE is a method used to determine the expression rates of a gene controlled by two opposing general transcription factors [17, 18]. In this case, we use this operator to obtain the expression rate of pTie2 in response to the two opposing factors Ang1 and Ang2. These factors compete to bind one of n common Tie2 sites with two separate binding affinities. Considering a group of $n = 4$ Tie2 receptors, activation is possible only if a tetramer of Ang1 binds to 4 Tie2 or when a tetramer of Ang2 binds to 4 Tie2.

Assumption 1. *Since Ang2 exists in both dimeric (75%), trimeric (16%), and tetrameric (9%) forms, to avoid inflating the model with three different forms of Ang2, we assume that only the dimeric form of Ang2 is present and that 9% of its concentration leads to Tie2 activation, while the remaining concentration does not.*

Thus, we define the operators

$$Z^{(n)}(j_1, j_2) := \frac{n!}{j_1! j_2! j_0!} \, \text{Ang1} \, \text{Ang2} \left(\frac{\text{Tie2}}{K_1} \right)^{j_1} \left(\frac{\text{Tie2}}{K_2} \right)^{j_2}$$

with $j_0 = n - j_1 - j_2$, $j_1 = 0, 1, 2, 3, 4$, $j_2 = 0, 1, 2$, and K_1 and K_2 being Ang1-Tie2 and Ang2-Tie2 affinity constants, respectively, such that $K_i = k_{-i}/k_i$. Moreover, defining

$$M_4 := \frac{9}{100} \sum_{l=0}^{2} Z^{(4)}(j_1 = l, j_2 = 2) , \qquad M_3 := \frac{16}{100} \sum_{l=0}^{2} Z^{(4)}(j_1 = l, j_2 = 2) , \quad M_2 := \frac{75}{100} \sum_{l=0}^{2} Z^{(4)}(j_1 = l, j_2 = 2)$$

the fractions of the operator for Ang2 that account for the effects of its tetramer, trimer, and dimer forms (in their corresponding percentages), we get

$$G(\text{Ang1}, \text{Ang2}, \text{Tie2}) = \frac{Z^{(4)}(j_1 = 4, j_2 = 0) + M_4}{\sum_{j_1 + j_2 \leq 4} Z^{(4)}(j_1, j_2)} . \tag{12}$$

In modeling the growth rate function $N(R)$, we incorporate a density-dependent effect: the growth rate increases for low values of R, indicating a higher availability of free receptors for ligand binding. Conversely, the growth rate decreases as R increases, reflecting a reduction in the availability of free receptors. This phenomenon is analogous to well-known ecological models, such as the Allee effect [19]. Specifically, at low R densities, there is a high level of free receptors available for ligand binding, which enhances the growth rate. In contrast, higher R densities indicate a lower level of free receptors, reducing the likelihood of tetrameric Ang1 binding and thus activating phosphorylation, leading to a decrease in the growth rate. Taking this into account, we approximate $N(R)$ with the following function

$$N(R) = \left(k_R \left(1 - \frac{R}{K_R} \right) - \frac{m}{R + b} \right) \tag{13}$$

where k_R refers to the phosphorylation rate, K_R to the carrying capacity, b is the semi-saturation constant, and m is the maximum consumption rate. In order to ensure the existence of two real roots for the equation $N(R) = 0$, we have to impose that $k_R \geq 4K_R/(b+K_R)^2$. Moreover, if $b \geq \max\{K_R, m/k_R\}$ or $m/k_R \leq b \leq K_R$ (when $K_R \geq m/k_R$), then a weak Allee effect is recovered, while if $b \leq \min\{K_R, m/k_R\}$ we obtain a strong Allee effect. No positive roots can be obtained when $K_R \leq b \leq m/k_R$ and $K_R \leq m/k_R$ [19]. Using (12) and (13) in (11), and the latter in (9) and (10), we obtain the equation describing the dynamical evolution of R and pTie2, respectively.

S.2 VEGF module

In the VEGF module, we describe the activation of VEGF receptors upon binding/dimerization by VEGF. Specifically, we model the interaction between VEGF ligands and VEGFR that leads to receptor dimerization and its activation. In the VEGF/VEGFR system, the ligand is bivalent, indicating that one VEGF molecule binds to two VEGFR receptors. Conversely, each VEGFR receptor can bind to a single VEGF molecule. The complex (VEGF(VEGFR)2) is formed by two VEGFR receptors and one VEGF molecule. This complex formation is essential for the phosphorylation of the receptor and subsequent activation of downstream pathways. Precisely, the VEGF module takes the following variables into account.

- VEGF (V) ligand is present in a dimeric form, and it binds to the VEGFR receptor. The dimerization of the receptor is the fundamental mechanism that activates the underlying pathway. VEGF molecules are produced by tumor cells in hypoxic conditions to attract endothelial cells, thereby directing nutrients and oxygen toward the hypoxic sites.
- VEGFR (u) receptor is expressed on the membrane of endothelial cells, and it binds to VEGF to activate the underlying signaling pathway through receptor dimerization.
- (VEGF(VEGFR)2) (b) is the dimer complex VEGF-VEGFR formed by the dimeric form of VEGF and a cluster of two VEGFR receptors.
- The variable x represents dVEGFR, which is the dimerized form of VEGFR responsible for VEGF signaling.

Observation 1. *We assume that the total number of Tie2 and VEGF receptors remains constant at any given location and time. This assumption is supported in part by observations from [20] regarding Tie2 expression in tumors over time. However, in reality, the concentrations of VEGFR and Tie2 can vary significantly in many cases. Following the approach in [21], we adopt this model assumption to make the model more tractable and manageable in complexity.*

Following the framework proposed in [3] for this intracellular signaling cascade, we describe the evolution of the dynamics with the following ODE system:

$$\begin{cases} \dfrac{dV}{dt} = k_V h_{1,V}(O_2) h_{2,V}(\mathrm{PI}) C - k_{\mathrm{on}} V u - d_V V \\ \dfrac{du}{dt} = k_{\mathrm{off}}\, b - k_{\mathrm{on}} V u + k^x_{\mathrm{off}}\, x - k^x_{\mathrm{on}} \pi\, \Delta^2 \rho u b \\ \dfrac{db}{dt} = -k_{\mathrm{off}}\, b + k_{\mathrm{on}} V u + k^x_{\mathrm{off}}\, x - k^x_{\mathrm{on}} \pi \Delta^2 \rho u b \\ \dfrac{dx}{dt} = -k^x_{\mathrm{off}}\, x + k^x_{\mathrm{on}} \pi \Delta^2 \rho u b\,. \end{cases} \tag{14}$$

Here, the parameters are defined as follows: k_V and d_V represent the constant hypoxic cell-induced production and natural decay rate of VEGF, respectively; k_{on} and k_{off} are the binding and unbinding rates between V and u; k^x_{on} and k^x_{off} are the cross-link formation (dimerization) and dissociation constants. Moreover, Δ represents a characteristic distance of the ligand–receptor heterodimer, while ρ is the receptor surface density.

System (14) is supplemented by an equation that describes the evolution of the concentration of VEGF. To this end, we propose a model that incorporates the effects of (lack of) oxygen and PARP inhibitors on VEGF production. Experimental evidence, such as the one in Figure 3 of [2], suggests that VEGF secretion is oxygen-dependent, since it increases as the oxygen concentration decreases. This effect is included in the model using the function $h_{1,V}(O_2)$, represented in the Supplementary Figure 2. In addition to the oxygen-dependent modulation of VEGF production, the model includes the function $h_{2,V}(\mathrm{PI})$ to account for the effects of PARP inhibitors on VEGF production. This is based on the observed reduction in VEGF expression over time when cells were treated with the PARP inhibitor PJ-34, as demonstrated in Figure 2H in [22]. The function $h_{2,V}(\mathrm{PI})$ is directly estimated from the results presented in [22].

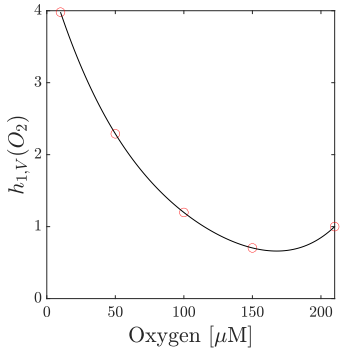

Supplementary Figure 2: **Oxygen-dependent VEGF expression.** Plot of the $h_{1,V}(O_2)$ function modeling the effect of oxygen concentration on VEGF expression. Red circles represent the experimental values taken from in [2].

S.3 Cellular module

The cellular module accounts for the evolution of the cellular populations (tumor and endothelial cells) and its regulation by changes in oxygen levels and cytokines released by the tumor.

- Tumor cells (C) experience proliferation regulated by oxygen levels and PARP inhibitors. Additionally, under highly hypoxic conditions, tumor cells release cytokines into the environment, which, paradoxically, become toxic to the tumor cells, resulting in cell death.
- Endothelial cells (ECs) proliferate in response to stimuli from VEGF and pTie2. Specifically, pTie2 plays a crucial role in regulating vessel wall stability: high levels of pTie2 stabilize the vessel wall, whereas low levels allow ECs to escape, initiating angiogenesis. Therefore, low levels of pTie2 are necessary to initiate angiogenesis. Additionally, angiogenesis requires high levels of dimerized VEGFR (x). If pTie2 levels permit angiogenesis but the VEGF stimulus is insufficient to promote EC proliferation, the newly formed vessels collapse under tumor pressure [23, 24]. Conversely, high levels of dimerized VEGFR allow for angiogenesis to occur. This creates a dual feedback loop between the VEGF-VEGFR and Tie-Ang signaling pathways. Furthermore, we assume that vessel collapse mechanisms may be common in newly formed vessels where EC density is not close to its carrying capacity (K_E). For EC densities approximately equal to K_E, vessels are considered sufficiently stable to suppress collapse.
- Oxygen (O_2) is generated by endothelial cells (ECs) and serves as a nutrient source for tumor cells, which, in turn, consume it.
- Cytokines (Cyt) play various roles in the tumor microenvironment, and their functions depend on their structure and type. They are classified into different superfamilies, including interferons (IFNs), interleukins (ILs), tumor necrosis factors (TNFs), and transforming growth factors (TGFs) [25]. Here, we focus on specific types of cytokines that are produced by tumor cells in response to low levels of oxygen [26]. These cytokines contribute to tumor cell necrosis, as they induce an inflammatory response.

The evolution of their dynamics is described by the following system of ordinary differential (ODE) equations:

$$\begin{cases} \dfrac{dC}{dt} = h_{1,C}(O_2)h_{2,C}(\mathrm{PI})C\left(1-\dfrac{C}{K_C}\right) - d_C C\, Cyt \\ \dfrac{dE}{dt} = h_{1,E}\left(\mathrm{pTie2}, x\right) h_{2,E}(\mathrm{PI})E\left(1-\dfrac{E}{K_E}\right) \\ \dfrac{dO_2}{dt} = k_{O_2,p}E - k_{O_2,c}C\, O_2 - d_{O_2}O_2 \\ \dfrac{dCyt}{dt} = k_{Cyt}\dfrac{C}{O_2} - d_{Cyt}Cyt\,. \end{cases} \tag{15}$$

Here, d_C, d_{O_2}, and d_{Cyt} represent the constant decay/death rates for tumor, oxygen, and cytokines, respectively. $k_{O_2,c}$ denotes the oxygen consumption rate due to tumor cells, while $k_{O_2,p}$ and k_{Cyt} stand for the constant production rate of oxygen (by ECs) and cytokines (by tumor cells), respectively. Specifically, k_{Cyt} has the non-zero value reported in the Supplementary Table 2 only when O_2 falls below 5%, while its value is set to 0 above this threshold. Logistic growth is considered for both tumor and endothelial cells, reaching their respective carrying capacities K_C and K_E. The growth rates depend on the dynamics of oxygen, Tie-Ang, and

VEGF-VEGFR signaling pathways. The function $h_{1,C}(O_2)$ models oxygen-dependent tumor cell proliferation, with the proliferation rate being maximum and independent of O_2 for high oxygen levels. However, for low O_2 levels (below 5%, denoted as th_H), the tumor proliferation rate decreases with decreasing O_2 concentration [27, 28]. When the oxygen level drops below 1%=: th_{SH} (severe hypoxia), tumor cells initiate a process of cell death. This behavior is captured by assuming that is

$$h_{1,C}(O_2) = \begin{cases} k_C & O_2 \geq th_H \\ \\ k_C \tanh\left[\alpha\left(O_2 - th_{SH}\right)\right] & \text{otherwise} \end{cases} \tag{16}$$

where k_C is the constant tumor proliferation rate in normoxic situations, and α is a constant coefficient that ensures the continuity of $h_{1,C}(O_2)$ at th_H. On the other hand, $h_{1,E}\left(\text{pTie2}, x\right)$ accounts for the effect of both pTie2 and dVEGFR signaling on EC proliferation. Specifically, we assume that

$$h_{1,E}\left(\text{pTie2}, x\right) = k_E(\text{pTie2}) \tanh\left(x^*(V) - th_x\right) \tag{17}$$

where x^* is the quasi-equilibrium state for the dimerized (active) VEGFR, whose levels depend on the concentration of VEGF, while th_x is the threshold of VEGF stimuli on ECs determining vessel collapsing ($x^* < th_x$) or vessel formation ($x^* \geq th_x$). $k_E(\text{pTie2})$, instead, accounts for pTie2 role on ECs proliferation: high levels of pTie2 inhibit angiogenesis, while endothelial cell dynamics are allowed for low pTie2 levels. In particular

$$k_E(\text{pTie2}) = k_E \, \frac{(th_{\text{pTie2}})^p}{((th_{\text{pTie2}})^p + (\text{pTie2})^p)}$$

with k_E constant endothelial cell growth rate and th_{pTie2} threshold of pTie2 levels allowing for vessel stability. The exponent p can be used to make more or less sharp the transition between angiogenesis promotion ($\text{pTie2} > th_{\text{pTie2}}$) or inhibition ($\text{pTie2} < th_{\text{pTie2}}$). For the simulations reported here, we consider a sharp transition by setting $p = 100$. Finally, when PARP inhibitors are included in the setting, then we account for their effect on tumor and endothelial cell proliferation through the functions $h_{2,C}(\text{PI})$ and $h_{2,E}(\text{PI})$, which take the simple form

$$h_{2,i}(\text{PI}) = \frac{1}{(1 + [\text{PI}])^{n_i}} \quad \text{for i=C, E}\,. \tag{18}$$

S.4 Summary of the model

Here, we present a summary of the developed model describing the interactions among the three distinct compartments outlined in Figure (1) of the main text: the angiopoietin compartment, the VEGF compartment, and the cellular compartment. In Supplementary Table 1 we summarize the independent variables of the model, their meaning, and units, while the definitions of the supplementary variables (R, $y_{i,j}$, z_i, r_i, and f_i for $i, j = 1, 2$) used in the equations have been previously provided in the corresponding sections.

Variable	Meaning	Unit
Ang1	free Angiopoietin 1 concentration	nM
(Ang1(Tie2)4)	tetramer Ang1-Tie2 complex concentration	nM
Ang2	free Angiopoietin 2 concentration	nM
(Ang2(Tie2)2)	dimer Ang2-Tie2 complex concentration	nM
Tie2	free Tie2 concentration	nM
pTie2	phosphorylated Tie2 concentration	nM
V	free VEGF concentration	nM
u	unbound VEGF receptor concentration	nM
b	bound VEGF receptor concentration	nM
x	dimerized VEGF receptor concentration	nM
C	tumor cell density	nM
E	endothelial cell density	nM
O_2	oxygen concentration	nM
Cyt	cytokines concentration	nM

Supplementary Table 1: Independent variables of system (19), their meaning, and their corresponding units of measure.

$$
\begin{cases}
\dfrac{d\,\mathrm{Ang1}}{dt} = -F_1 \\
\dfrac{d\,(\mathrm{Ang1(Tie2)4})}{dt} = F_1 \\
\dfrac{d\,\mathrm{Ang2}}{dt} = -F_2 + h_{\mathrm{Ang2}}(V)E - d_{\mathrm{Ang2}}\,\mathrm{Ang2} \\
\dfrac{d\,(\mathrm{Ang2(Tie2)2})}{dt} = F_2 \\
\dfrac{d\,\mathrm{Tie2}}{dt} = -4F_1 - 2F_2 \\
\dfrac{d\mathrm{pTie2}}{dt} = \dfrac{d\,\mathrm{Tie2}}{dt}\left[R - \dfrac{F(R)}{\sum\limits_{i=1}^{2}\left(d_i r_i (-1)^{i+1}(f_2 - f_1) - \dfrac{1}{r_i} z_i\, f + \dfrac{d\,f_i}{d\,A_{i,0}}\right)}\,\tilde{f}\right] \\
\dfrac{d\,V}{dt} = k_V h_{1,V}(O_2) h_{2,V}(\mathrm{PI}) C - k_{\mathrm{on}} V u - d_V V \\
\dfrac{d\,u}{dt} = k_{\mathrm{off}} b - k_{\mathrm{on}} V u + k^x_{\mathrm{off}} x - k^x_{\mathrm{on}} \pi \Delta^2 \rho u b \\
\dfrac{d\,b}{dt} = -k_{\mathrm{off}} b + k_{\mathrm{on}} V u + k^x_{\mathrm{off}} x - k^x_{\mathrm{on}} \pi \Delta^2 \rho u b \\
\dfrac{d\,x}{dt} = -k^x_{\mathrm{off}} x + k^x_{\mathrm{on}} \pi \Delta^2 \rho u b \\
\dfrac{d\,C}{dt} = h_{1,C}(O_2) h_{2,C}(\mathrm{PI}) C \left(1 - \dfrac{C}{K_C}\right) - d_C C\, Cyt \\
\dfrac{d\,E}{dt} = h_{1,E}\left(\mathrm{pTie2}, x\right) h_{2,E}(\mathrm{PI}) E \left(1 - \dfrac{E}{K_E}\right) \\
\dfrac{d\,O_2}{dt} = k_{O_2,p} E - k_{O_2,c} C\, O_2 - d_{O_2} O_2 \\
\dfrac{d\,Cyt}{dt} = k_{Cyt} \dfrac{C}{O_2} - d_{Cyt} Cyt\,.
\end{cases}
\tag{19}
$$

Supplementary Note 2: Parameter estimation

In this section, we collect the parameter values used in system (19) and detailed in Supplementary Table 2, alongside with the reference values (listed in Supplementary Table 5) used for non-dimensionalization, as described in Supplementary Note 3. The parameter estimates are derived from various literature sources. Specifically, for the angiopoietin module, we primarily refer to [29], where estimations for binding/unbinding rates (k_1, k_{-1}, k_2, k_{-2}) of Ang1 and Ang2, as well as production (k_{Ang2}) and decay (d_{Ang2}) rates of Ang2, are provided based on previous experimental and mathematical studies [30, 31, 21] and considering their interactions with the VEGF-VEGFR pathway. Estimations for VEGF-related parameters (production k_V, decay d_V rates) are also provided in [29], calibrated to account for their interactions with the angiopoietin dynamics. The ratio R assumes a carrying capacity $K_R = 1$, implying phosphorylation of all Tie2 receptors. Phosphorylation (k_R) and decay (d_R) rates are derived from [32], which extensively models this signaling pathway. Parameters m and b are calibrated using the Ang-Tie2 module to align the *in-silico* results with the findings in [7]. For VEGF-VEGFR parameters (k_{off}, k_{on}, k^x_{off}, k^x_{on}, Δ, ρ), we refer to [3], where the VEGF-VEGFR model was firstly introduced, ensuring parameter estimations are consistent with those proposed in [29]. Estimations for endothelial cell parameters (k_E, th_{pTie2}, th_x) are adopted from [29] for internal consistency. Oxygen-related parameters ($k_{O_{2,p}}$, $k_{O_{2,c}}$, d_{O_2}) are sourced from [33, 34], which provide suitable estimations from experimental data. The tumor proliferation rate is selected to reflect an approximate doubling time of ≈ 1 day, typical for various solid tumors, while cell carrying capacities are set sufficiently high to prevent cells from reaching this limit during transient phases characterized by cyclic hypoxia dynamics. Finally, cytokine-related parameters (d_C, k_{Cyto}, d_{Cyto}) are estimated based on an average of different values reported in [35], mainly focusing on Interleukin-27 (IL-27), which is secreted by tumor cells, activates immune responses, and influences tumor outcomes.

In order to provide support to the robustness of our results, we have run a sensitivity analysis on some of the parameters that were not available from experiments related to the specific setting under investigation. Precisely, we analyze the model response to variation in b, m, d_C, k_{Cyt}, and d_{Cyt}. Assuming θ to be the parameter under investigation and given θ_B its baseline value, we consider equally distributed points in the range $[\theta_B - \theta_B/2, \theta_B + \theta_B/2]$. The effects of the variation of the parameter $\theta \in \{m, b\}$ on the results shown in Figure 2 of the manuscript are collected in the Supplementary Figure 3.

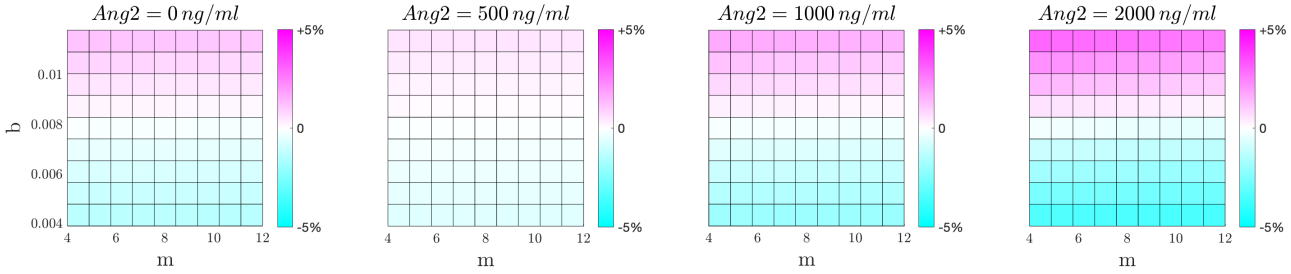

Supplementary Figure 3: **Sensitivity analysis on P/T ratio.** Percentage variations $\mathbb{V}$ in the P/T (phosphorylated/total Tie2) ratio are reported for different values of m and b within a range $\pm 50\%$ with respect to their baseline estimations.

We indicate with $\mathbb{V}$ the percentage variation defined as

$$\mathbb{V} := \frac{\mathbf{X}_B - \mathbf{X}_V}{\mathbf{X}_B} \cdot 100$$

where $\mathbf{X}_B$ represent the value of the observable $\mathbf{X}$ when the baseline value for the parameters are used, while $\mathbf{X}_V$ the one obtained varying the parameter values. We notice that the biggest variations are observed for the highest Ang2 initial concentration. However, the variations remain in a range of $\pm 5\%$ with respect to the results obtained with the baseline parameter value. Considering, instead, the qualitative evolution of our system shown in Figures 3 and 4 of the main manuscript, we analyze the effect of varying the parameters $\theta \in \{m, b, d_C, k_{Cyt}, d_{Cyt}\}$ on the dynamics. To be precise, for the results in Figure 3 we let vary all the five parameters, while for the ones in Figure 4 we only reported the effects of variations in b and m, as we showed that the feedback loop between tumor cells, oxygen, and cytokines (and, thus, the parameter involved in cytokine dynamics) drive the emergence and evolution of the cyclic hypoxia. Therefore, in the advanced-stage scenario, the dynamics would be clearly influenced by d_C, k_{Cyt}, and d_{Cyt} variations. Results of these analyses are reported in the Supplementary Tables 3 and 4. Precisely, here the maximum percentage variation is defined as

$$\mathcal{V}_{\%} := \max_{t \in [0,T]} \mathbb{V}(t)$$

with $T = 90\,d$ the final temporal point of the numerical simulations and $\mathbb{V}(t)$ the vector with the percentage variation at each time step. $\underline{\theta} := \theta_B - \theta_B/2$ represents the minimum parameter value used for the analysis, while

Parameter	Description	Value [unit]	Source
k_1	Ang1-Tie2 binding rate	$0.116 \cdot 10^{-3}$ $[(\text{nM}\cdot\text{s})^{-1}]$	[29]
k_{-1}	Ang1-Tie2 unbinding rate	$0.16 \cdot 10^{-3}$ $[\text{s}^{-1}]$	[29]
k_2	Ang2-Tie2 binding rate	$0.116 \cdot 10^{-3}$ $[(\text{nM}\cdot\ \text{s})^{-1}]$	[29]
k_{-2}	Ang2-Tie2 unbinding rate	$0.35 \cdot 10^{-3}$ $[\text{s}^{-1}]$	[29]
k_{Ang2}	Ang2 production rate by ECs	$1.23 \cdot 10^{-3}$ $[\text{s}^{-1}]$	[29]
d_{Ang2}	Ang2 degradation rate	$0.12 \cdot 10^{-4}$ $[\text{s}^{-1}]$	[29]
m	R maximum consumption rate	8	(*)
b	R semi-saturation constant	0.01	(*)
K_R	R carrying capacity	1	(*)
k_R	R phosphorylation rate	0.096 $[(\text{nM}\cdot\text{s})^{-1}]$	[32] (*)
d_R	R decay rate	0.000684 $[\text{s}^{-1}]$	[32] (*)
k_V	VEGF production rate	$3.09 \cdot 10^{-4}$ $[(\text{nM}\cdot\text{s})^{-1}]$	[29]
d_V	VEGF degradation rate	$1.81 \cdot 10^{-4}$ $[\text{s}^{-1}]$	[29]
k_{off}	VEGF-VEGFR unbinding rate	$0.42 \cdot 10^{-3}$ $[\text{s}^{-1}]$	[3]
k_{on}	VEGF-VEGFR binding rate	$0.69 \cdot 10^{-3}$ $[(\text{nM}\cdot\text{s})^{-1}]$	[3]
k^x_{off}	cross-link dissociation rate	10^{-3} $[\text{s}^{-1}]$	[3]
k^x_{on}	cross-link association rate	$4.16 \cdot 10^{3}$ $[\text{s}^{-1}]$	[3]
Δ	distance of the ligand–receptor heterodimer	0.0025 $[\mu\text{m}]$	[3]
ρ	receptor surface density	50 $[\mu\text{m}^{-2}]$	[3]
K_C	tumor carrying capacity	$10C_0$ [nM]	(*)
k_C	tumor growth rate	10^{-6} $[\text{s}^{-1}]$	[36]
d_C	cytokines-mediated tumor death rate	$1.16 \cdot 10^{-6}$ $[(\text{nM}\cdot\text{s}\ )^{-1}]$	[35] (*)
K_E	EC carrying capacity	$10E_0$ [nM]	(*)
k_E	EC growth rate	$1.74 \cdot 10^{-5}$ $[\text{s}^{-1}]$	[29]
th_{pTie2}	threshold for vessel stability	0.49 [nM]	[29]
th_x	threshold for vessel remodelling	0.665 [nM]	[29]
$k_{O_{2,p}}$	oxygen supply rate	$3.9 \cdot 10^{-6}$ $[\text{s}^{-1}]$	[33]
$k_{O_{2,c}}$	oxygen consumption rate	$0.69 \cdot 10^{-6}$ $[(\text{nM}\ \text{s})^{-1}]$	[33]
d_{O_2}	oxygen decay rate	$0.8 \cdot 10^{-5}$ $[\text{s}^{-1}]$	[34]
th_{H}	normoxia/hypoxia threshold	$5\%\, O_2$	[27, 28]
th_{SH}	hypoxia/severe hypoxia threshold	$1\%\, O_2$	[27, 28]
k_{Cyt}	cytokine production rate	$0.123 \cdot 10^{-7}$ $[(\text{nM}\cdot\text{s})^{-1}]$	[35] (*)
d_{Cyt}	cytokine decay rate	$0.61 \cdot 10^{7}$ $[\text{s}^{-1}]$	[35] (*)

Supplementary Table 2: Estimation of the model parameters involved in system (19). (*) indicates that the corresponding parameter value has been estimated from the data provided in this work or adapted from ranges reported in the literature, as detailed explained in Supplementary Note 2.

$\widehat{\theta} := \theta_B + \theta_B/2$ represents the maximum value used for the analysis. We reported the results for tumor cells and oxygen only, as these are the variables of greater interest for the qualitative system dynamics. However, comparable results can be obtained also for the other involved agents. Finally, referring to the results collected in Figures 6 and 7 of the main manuscript, only the one concerning the effects of PARP inhibitors on VEGF production (Figure 6A) could be impacted by variation in the considered parameters, namely in d_C, k_{Cyt}, and d_{Cyt}. However, with a similar analysis of the percentage variation we did not notice any relevant difference. The absolute value of the percentage variation never goes above 10^{-6}. This is because the simulations that give rise to the results in Figure 6A are run for no longer than 24h, a much shorter time window with respect to the typical time of evolution of the cycles of hypoxia, on which the effect of the variation in these parameters is

$\mathbf{X}$ \ θ	$\underline{m}$	$\widehat{m}$	$\underline{b}$	$\widehat{b}$	$\underline{d}_C$	$\widehat{d}_C$	$\underline{k}_{Cyt}$	$\widehat{k}_{Cyt}$	$\underline{d}_{Cyt}$	$\widehat{d}_{Cyt}$
C	-0.94%	-0.98%	-0.96%	-0.96%	-9.8%	5.6%	-9.8%	5.6%	4.4%	2.7%
O_2	0.95%	0.93%	0.94%	0.94%	8.5%	-5.6%	8.5%	-5.5%	-4.4%	-2.5%

Supplementary Table 3: Maximum percentage variations in the evolution of tumor cells C and oxygen O_2 in the early-stage tumor scenario are reported when varying the value of $\theta \in \{m, b, d_C, k_{Cyt}, d_{Cyt}\}$. Precisely, $\underline{\theta} := \theta_B - \theta_B/2$ and $\widehat{\theta} := \theta_B + \theta_B/2$ represent the minimum and maximum parameter values used in the analysis.

$\mathbf{X}$ \ θ	$\underline{m}$	$\widehat{m}$	$\underline{b}$	$\widehat{b}$
C	-0.07%	0.07%	0.003%	-0.003%
O_2	-0.12%	0.13%	0.005%	-0.005%

Supplementary Table 4: Maximum percentage variations obtained in the evolution of tumor cells C and oxygen O_2 in the advanced-stage tumor scenario when varying the value of $\theta \in \{m, b\}$. Precisely, $\underline{\theta} := \theta_B - \theta_B/2$ and $\widehat{\theta} := \theta_B + \theta_B/2$ represent the minimum and maximum parameter values used in the analysis.

instead relevant. Overall with these analyses, we can ensure the robustness of our results for variations of the parameters for which there were not available precise estimations from the literature or from the experiments.

Supplementary Note 3: Model non-dimensionalization

System (19) integrates molecular-level processes (related to Ang-Tie2 and VEGF-VEGFR signaling pathways) with population-level dynamics (related to oxygen, cytokines, and cell evolution), which operate on distinct temporal scales. To accommodate these variations, we adopt a non-dimensionalized version of the model. Precisely, we rescale the model variables with respect to their initial conditions and the time variable. These initial values correspond to physiological levels for the different components and are reported in the Supplementary Table 5.

Parameter	Value [unit]	Source
$A_{1,0}$	0.358 [nM]	[7]
$A_{2,0}$	[0-7.16] [nM]	[7]
$(\text{Ang1(Tie2)4})_0$	0.0179 [nM]	(*)
$(\text{Ang2(Tie2)2})_0$	0.0179 [nM]	(*)
Tie2_0	1 [nM]	[29]
pTie2_0	0.17 [nM]	(*)
V_0	3.33 [nM]	[29]
u_0	7.64 [nM]	[29]
b_0	2.67 [nM]	(*)
x_0	0.53 [nM]	(*)
C_0	1 [nM]	(*)
E_0	1 [nM]	(*)
$O_{2,0}$	210 [μM]	[27]
Cyt_0	0.36 $\cdot 10^{-3}$ [nM]	[35]

Supplementary Table 5: Reference values for the different agents involved in system (19). (*) indicates that the corresponding parameter value has been estimated from the data provided in this work or adapted from ranges reported in the literature, as detailed explained in the Supplementary Note 2.

To not overload the notation, we use the same name for rescaled variables, i.e.,

$$\text{Ang1} := \frac{\text{Ang1}}{A_{1,0}}, \qquad (\text{Ang1(Tie2)4}) := \frac{(\text{Ang1(Tie2)4})}{(\text{Ang1(Tie2)4})_0}, \qquad (\text{Ang2(Tie2)2} := \frac{(\text{Ang2(Tie2)2})}{(\text{Ang2(Tie2)2})_0},$$

$$\text{Ang2} := \frac{\text{Ang2}}{A_{2,0}}, \qquad \text{Tie2} := \frac{\text{Tie2}}{\text{Tie2}_0}, \qquad \text{pTie2} := \frac{\text{pTie2}}{\text{pTie2}_0}, \quad \text{V} := \frac{\text{V}}{V_0}, \qquad u := \frac{u}{u_0},$$

$$b := \frac{b}{b_0}, \qquad x := \frac{x}{x_0}, \qquad C := \frac{C}{K_C}, \qquad E := \frac{E}{K_E}, \qquad O_2 := \frac{O_2}{O_{2,0}}, \qquad Cyt := \frac{Cyt}{Cyt_0}.$$

We notice that R, whose evolution is given by (6), is already non-dimensionalized, as well as $y_{i,j}$ and z_i, for $i, j = 1, 2$. By rescaling the temporal variable as

$$\tau = t\, k_{-1},$$

the dynamics of the angiopoietin module given by system (1) and equations (6) and (10) reads

$$
\begin{cases}
\dfrac{d\,\mathrm{Ang1}}{d\tau} = \delta_1(\mathrm{Ang1.Tie2})4 - \alpha_1 \mathrm{Ang1}\cdot \mathrm{Tie2}^4 \\
\dfrac{d\,(\mathrm{Ang1(Tie2)4})}{d\tau} = \dfrac{\alpha_1}{\delta_1}\mathrm{Ang1}\cdot \mathrm{Tie2}^4 - (\mathrm{Ang1(Tie2)4}) \\
\dfrac{d\,\mathrm{Ang2}}{d\tau} = \delta_2\alpha_{-2}(\mathrm{Ang2.Tie2})2 - \alpha_2 \mathrm{Ang2}\cdot \mathrm{Tie2}^2 + h_{\mathrm{Ang2}}(V)E - \bar{d}_{A_2}\mathrm{Ang2} \\
\dfrac{d\,(\mathrm{Ang2(Tie2)2})}{d\tau} = \dfrac{\alpha_2}{\delta_2}\mathrm{Ang2}\cdot \mathrm{Tie2}^2 - \alpha_{-2}(\mathrm{Ang2(Tie2)2}) \\
\dfrac{d\,\mathrm{Tie2}}{d\tau} = \delta_1\gamma_1(\mathrm{Ang1(Tie2)4}) - \alpha_1\gamma_1\mathrm{Ang1}\cdot \mathrm{Tie2}^4 + \alpha_{-2}\gamma_2\delta_2(\mathrm{Ang2(Tie2)2}) - \alpha_2\gamma_2\mathrm{Ang2}\cdot \mathrm{Tie2}^2 \\
\dfrac{dR}{d\tau} = -\dfrac{F(R)}{\sum\limits_{i=1}^{2}\left(d_i r_i(-1)^{i+1}(f_2-f_1) - \dfrac{1}{r_i}z_i\,f + \dfrac{d\,f_i}{d\,A_{i,0}}\right)} f\,\dfrac{d\mathrm{Tie2}}{d\tau} \\
\dfrac{d\mathrm{pTie2}}{d\tau} = \gamma_3\dfrac{d\mathrm{Tie2}}{d\tau}\left[R - \dfrac{F(R)}{\sum\limits_{i=1}^{2}\left(d_i r_i(-1)^{i+1}(f_2-f_1) - \dfrac{1}{r_i}z_i\,f + \dfrac{d\,f_i}{d\,A_{i,0}}\right)}\tilde{f}\right].
\end{cases}
\tag{20}
$$

The rescaled parameters are defined as follows:

$$
\alpha_1 = \frac{k_1}{k_{-1}}(\mathrm{Tie2}_0)^4\,, \qquad \alpha_2 = \frac{k_2}{k_{-1}}(\mathrm{Tie2}_0)^2\,, \qquad \alpha_{-2} = \frac{k_{-2}}{k_{-1}}\,, \qquad \delta_1 = \frac{(\mathrm{Ang1(Tie2)4})_0}{A_{1,0}}\,, \qquad \bar{d}_{A_2} := \frac{d_{\mathrm{Ang2}}}{k_{-1}}\,,
$$

$$
\gamma_1 = 4\,\frac{A_{1,0}}{\mathrm{Tie2}_0}\,, \quad \gamma_2 = 2\,\frac{A_{2,0}}{\mathrm{Tie2}_0}\,, \quad \gamma_3 = \frac{\mathrm{Tie2}_0}{\mathrm{pTie2}_0}\,, \qquad \bar{k}_{\mathrm{Ang2}} = \frac{k_{\mathrm{Ang2}}}{k_{-1}}\frac{K_E}{A_{2,0}}\,, \qquad \delta_2 = \frac{(\mathrm{Ang2(Tie2)2})_0}{A_{2,0}}\,.
$$

For the VEGF module described with system (14), the non-dimensionalized dynamics reads

$$
\begin{cases}
\dfrac{d\,V}{d\tau} = \bar{k}_V\,h_{1,V}(O_2)h_{2,V}(PI)C - \bar{k}_{\mathrm{on}}Vu - \bar{d}_V V \\
\dfrac{d\,u}{d\tau} = \bar{k}_{\mathrm{off}}\,\gamma_b\,b - \bar{k}_{\mathrm{on}}\,\gamma_V\,V\,u + \bar{k}^x_{\mathrm{off}}\,\gamma_x\,x - \bar{k}^x_{\mathrm{on}}\,\pi\,\Delta^2\,\gamma_b\,\rho\,u\,b \\
\dfrac{d\,b}{d\tau} = -\bar{k}_{\mathrm{off}}\,b + \bar{k}_{\mathrm{on}}\,\dfrac{\gamma_V}{\gamma_b}\,V\,u + \bar{k}_{\mathrm{off}}\,\dfrac{\gamma_x}{\gamma_b}^{\,x}\,x - \bar{k}^x_{\mathrm{on}}\,\pi\,\Delta^2\,\rho\,u\,b \\
\dfrac{d\,x}{d\tau} = -\bar{k}^x_{\mathrm{off}}\,x + \bar{k}^x_{\mathrm{on}}\,\dfrac{\gamma_b}{\gamma_x}\,\pi\,\Delta^2\,\rho\,u\,b\,.
\end{cases}
\tag{21}
$$

Here, the rescaled parameters are defined as follows:

$$
\bar{k}_{\mathrm{on}} = \frac{k_{\mathrm{on}}}{k_{-1}}u_0\,, \qquad \bar{k}_{\mathrm{off}} = \frac{k_{\mathrm{off}}}{k_{-1}}\,, \qquad \bar{k}^x_{\mathrm{on}} = \frac{k^x_{\mathrm{on}}}{k_{-1}}\,u_0\,, \qquad \bar{k}^x_{\mathrm{off}} = \frac{k^x_{\mathrm{off}}}{k_{-1}}\,,
$$

$$
\bar{k}_V = \frac{k_V}{k_{-1}}\frac{K_C}{V_0}\,, \qquad \bar{d}_V = \frac{d_V}{k_{-1}}\,, \qquad \gamma_x = \frac{x_0}{u_0}\,, \qquad \gamma_V = \frac{V_0}{u_0}\,, \qquad \gamma_b = \frac{b_0}{u_0}\,.
$$

Finally, the non-dimensionalized version of the cellular module described in system (15) reads

$$
\begin{cases}
\dfrac{d\,C}{d\tau} = h_{1,C}(O_2)h_{2,C}(\mathrm{PI})C\,(1-C) - \bar{d}_C C\,Cyt \\
\dfrac{d\,E}{d\tau} = h_{1,E}\,(\mathrm{pTie2},x)\,h_{2,E}(\mathrm{PI})E\,(1-E) \\
\dfrac{d\,O_2}{d\tau} = \bar{k}_{O_2,p}E - \bar{k}_{O_2,c}C\,O_2 - \bar{d}_{O_2}O_2 \\
\dfrac{d\,Cyt}{d\tau} = \bar{k}_{Cyt}\dfrac{C}{O_2} - \bar{d}_{Cyt}Cyt
\end{cases}
\tag{22}
$$

with

$$\bar{d}_C = \frac{d_C}{k_{-1}} Cyt_0\,, \qquad \bar{k}_{O_2,p} = \frac{k_{O_2,p}}{k_{-1}} \frac{K_E}{O_{2,0}}\,, \qquad \bar{k}_{O_2,c} = \frac{k_{O_2,c}}{k_{-1}} K_M\,,$$

$$\bar{d}_{O_2} = \frac{d_{O,2}}{k_{-1}}\,, \qquad \bar{k}_{Cyt} = \frac{k_{Cyt}}{k_{-1}} \frac{K_C}{O_{2,0}}\,, \quad \bar{d}_{Cyt} = \frac{d_{Cyt}}{k_{-1}}\,.$$

The functions $h_{1,C}(O_2)$ and $h_{1,E}\,(\mathrm{pTie2}, x)$ are defined as in (16) and (17), respectively, with rescaled constant rates

$$\bar{k}_C = \frac{k_C}{k_{-1}} \quad \text{and} \quad \bar{k}_E = \frac{k_E}{k_{-1}}\,.$$

Moreover, the thresholds involved in these functions are also redefined as

$$th_{\bar{H}} = \frac{th_H}{O_{2,0}}\,, \qquad th_{\bar{SH}} = \frac{th_{SH}}{O_{2,0}}\,, \quad \text{and} \quad th_{\bar{x}} = \frac{th_x}{x_0}\,.$$

Supplementary Note 4: Additional figures

This section presents additional figures that complement the analysis discussed in the paper. In Supplementary Figure 4, we present the phase diagrams related to oxygen and endothelial cells (left plot), tumor cells (middle plot), and cytokines (right plot). These diagrams are derived numerically from the simulations depicted in Figure 4 of the main manuscript. Specifically, the three diagrams illustrate the emergence of a clear limit cycle in the system, indicative of sustained cycles of hypoxia over time. Our future plans include conducting a comprehensive analytical study of the proposed model. This study aims to explore the theoretical characterization of these fluctuations, providing deeper insights into their possible characteristics. Moreover, to remark on the consistency over time of the cyclic hypoxia, in Supplementary Figure 5 we include the corresponding time evolution for the four populations over a period of 180 days.

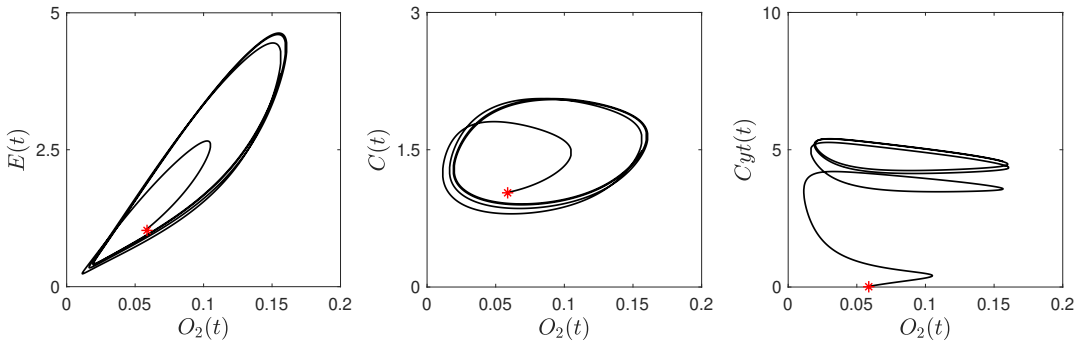

Supplementary Figure 4: **Limit cycle.** Phase diagrams of system (19) are presented for the parameter values specified in Supplementary Table 2, focusing on the advanced-stage tumor scenario. These diagrams illustrate the emergence of a limit cycle within the oxygen-cell-cytokines feedback loop, corresponding to sustained cyclic hypoxia. Left plot: oxygen-endothelial cells diagram. Middle plot: oxygen-tumor cells diagram. Right plot: oxygen-cytokines diagram.

Additionally, the Supplementary Figures 6 and 7 depict the initial stages of evolution of system (19) in early-stage and advanced-stage scenarios, respectively. The simulations span $t \in [0, T_0]$, where $T_0 = 0.27$ days. Given that we simulate the non-dimensionalized version of the model, the initial conditions for rescaled variables are uniformly set to 1, except for the cytokine population, which begins at zero due to normoxic conditions. During the initial stages of evolution, we observe a phenomenon of self-adaptation dynamics, whereby the different components of the model rapidly adjust their levels from their initial physiological states to coordinate with each other.

Supplementary References

1. Bogdanovic E, Nguyen VP, and Dumont DJ. Activation of Tie2 by angiopoietin-1 and angiopoietin-2 results in their release and receptor internalization. Journal of cell science 2006; 119:3551–60
2. Steinbrech DS, Mehrara BJ, Saadeh PB, Chin G, Dudziak ME, Gerrets RP, Gittes GK, and Longaker MT. Hypoxia regulates VEGF expression and cellular proliferation by osteoblasts in vitro. Plastic and reconstructive surgery 1999; 104:738–47
3. Alarcón T and Page KM. Mathematical models of the VEGF receptor and its role in cancer therapy. Journal of The Royal Society Interface 2007; 4:283–304
4. Kim KT, Choi HH, Steinmetz MO, Maco B, Kammerer RA, Ahn SY, Kim HZ, Lee GM, and Koh GY. Oligomerization and multimerization are critical for angiopoietin-1 to bind and phosphorylate Tie2. Journal of Biological Chemistry 2005; 280:20126–31
5. Davis S, Papadopoulos N, Aldrich TH, Maisonpierre PC, Huang T, Kovac L, Xu A, Leidich R, Radziejewska E, Rafique A, et al. Angiopoietins have distinct modular domains essential for receptor binding, dimerization and superclustering. Nature structural biology 2003; 10:38–44
6. Barton WA, Tzvetkova-Robev D, Miranda EP, Kolev MV, Rajashankar KR, Himanen JP, and Nikolov DB. Crystal structures of the Tie2 receptor ectodomain and the angiopoietin-2–Tie2 complex. Nature structural & molecular biology 2006; 13:524–32

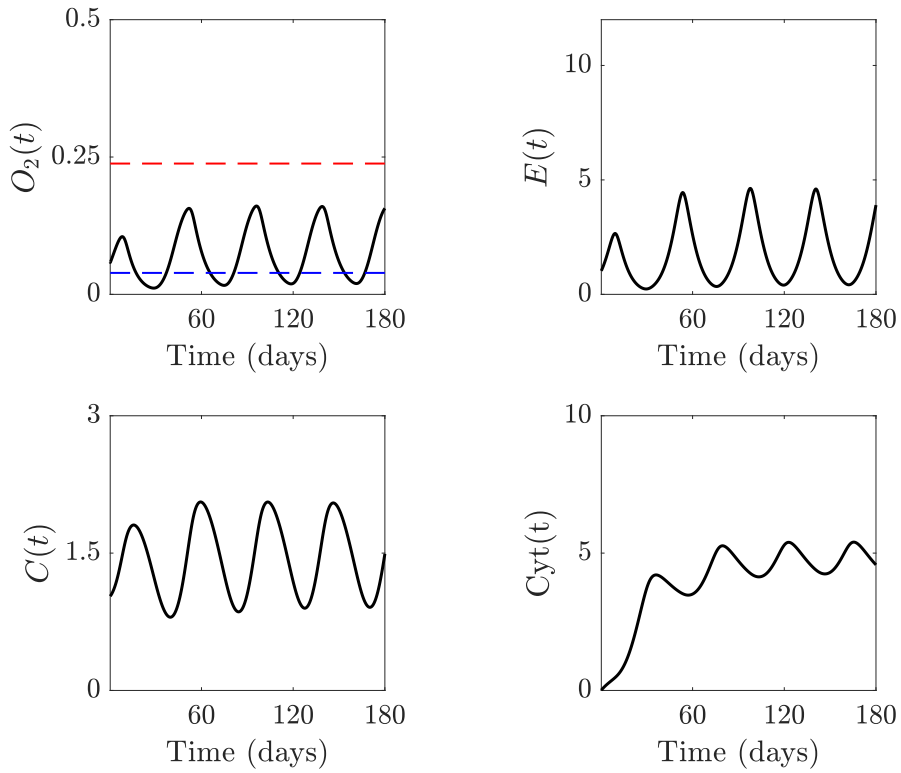

Supplementary Figure 5: **Sustained (over time) slow-cyclic hypoxia in advanced-stage tumor.** Qualitative results for oxygen, endothelial cells, tumor cells, and cytokines obtained from the evolution of system (19) for parameter values listed in Supplementary Table 2 are shown for the advanced-stage tumor case. The red and blue dashed line in the oxygen plot refers to normoxia-hypoxia (5% O_2) and hypoxia-severe hypoxia (1% O_2) thresholds, respectively. Simulations are run for 180 days to show how cyclic hypoxia is sustained over time. All the y-axis refer to non-dimensionalized densities or concentrations of the indicated agents.

7. Yuan HT, Khankin EV, Karumanchi SA, and Parikh SM. Angiopoietin 2 is a partial agonist/antagonist of Tie2 signaling in the endothelium. Molecular and cellular biology 2009; 29:2011–22
8. Yuan HT, Venkatesha S, Chan B, Deutsch U, Mammoto T, Sukhatme VP, Woolf AS, and Karumanchi SA. Activation of the orphan endothelial receptor Tie1 modifies Tie2-mediated intracellular signaling and cell survival. The FASEB Journal 2007; 21:3171–83
9. Kim HZ, Jung K, Kim HM, Cheng Y, and Koh GY. A designed angiopoietin-2 variant, pentameric COMP-Ang2, strongly activates Tie2 receptor and stimulates angiogenesis. Biochimica et Biophysica Acta (BBA)-Molecular Cell Research 2009; 1793:772–80
10. Oh H, Takagi H, Suzuma K, Otani A, Matsumura M, and Honda Y. Hypoxia and vascular endothelial growth factor selectively up-regulate angiopoietin-2 in bovine microvascular endothelial cells. Journal of Biological Chemistry 1999; 274:15732–9
11. Mandriota SJ and Pepper MS. Regulation of angiopoietin-2 mRNA levels in bovine microvascular endothelial cells by cytokines and hypoxia. Circulation research 1998; 83:852–9
12. Kelly BD, Hackett SF, Hirota K, Oshima Y, Cai Z, Berg-Dixon S, Rowan A, Yan Z, Campochiaro PA, and Semenza GL. Cell type–specific regulation of angiogenic growth factor gene expression and induction of angiogenesis in nonischemic tissue by a constitutively active form of hypoxia-inducible factor 1. Circulation research 2003; 93:1074–81
13. Mandriota SJ, Pyke C, Di Sanza C, Quinodoz P, Pittet B, and Pepper MS. Hypoxia-inducible angiopoietin-2 expression is mimicked by iodonium compounds and occurs in the rat brain and skin in response to systemic hypoxia and tissue ischemia. The American Journal of Pathology 2000; 156:2077–89
14. Teichert M, Milde L, Holm A, Stanicek L, Gengenbacher N, Savant S, Ruckdeschel T, Hasanov Z, Srivastava K, Hu J, et al. Pericyte-expressed Tie2 controls angiogenesis and vessel maturation. Nature communications 2017; 8:16106
15. Leppänen VM, Saharinen P, and Alitalo K. Structural basis of Tie2 activation and Tie2/Tie1 heterodimerization. Proceedings of the National Academy of Sciences 2017; 114:4376–81

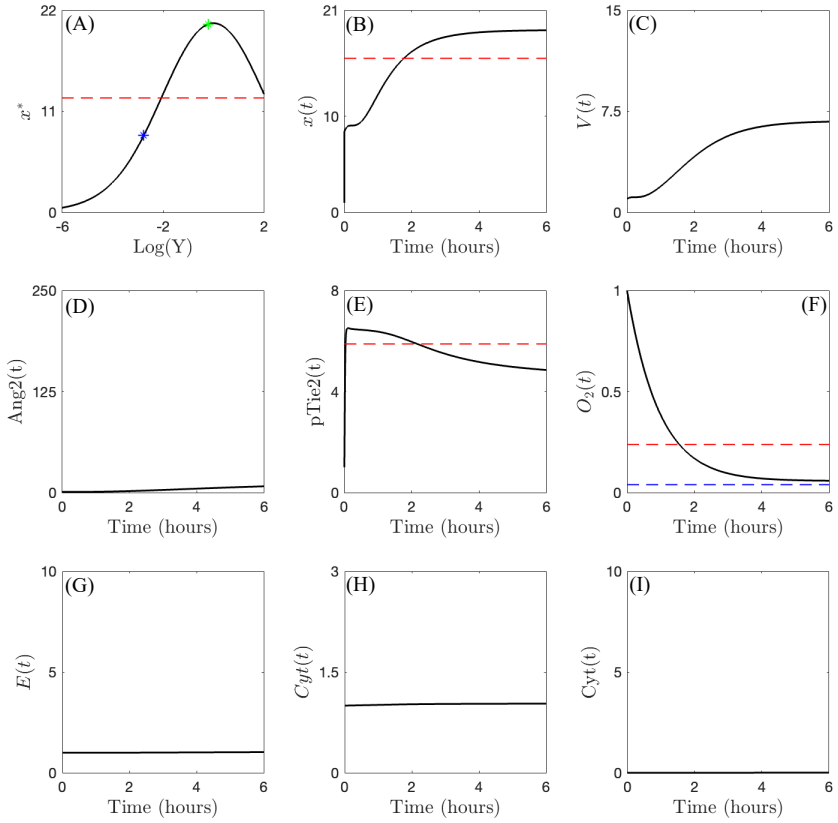

Supplementary Figure 6: **Early-stage tumor evolution.** Qualitative results of the evolution of the system (19) for parameter values listed in Supplementary Table 2 in the early-stage tumor scenario for $t \in [0, T_0]$ and $T_0 = 0.27$ days. (A) shows the qualitative relationship between Y and the equilibrium state of the dimerized form of VEGFR (x^*), i.e., x^* as a function of $Y := \frac{k_{\text{on}}}{k_{\text{off}}} V$, where k_{on} and k_{off} are the binding and unbinding rates between V and u, respectively [3]. The blue marker indicates the value of x^* for $V(0)$, while the green marker indicates the value of x^* at $V_{\max}$, which represents a numerically observed upper bound for the ligand concentration. Red dashed lines in (A) and (B) refer to the threshold th_x, above which EC proliferation is stimulated, the one in (E) plot to the threshold th_{pTie2}, below which vessel destabilization might happen, the red and blue in (F) refers to normoxia-hypoxia (5% O_2) and hypoxia-severe hypoxia (1% O_2) thresholds, respectively. All the y-axis refer to non-dimensionalized density or concentrations.

16. Gilman A and Arkin AP. Genetic "code": representations and dynamical models of genetic components and networks. Annual review of genomics and human genetics 2002; 3:341–69

17. Ackers GK, Johnson AD, and Shea MA. Quantitative model for gene regulation by lambda phage repressor. Proceedings of the national academy of sciences 1982; 79:1129–33

18. Shea MA and Ackers GK. The OR control system of bacteriophage lambda: A physical-chemical model for gene regulation. Journal of molecular biology 1985; 181:211–30

19. Taylor CM and Hastings A. Allee effects in biological invasions. Ecology Letters 2005; 8:895–908

20. Tse V, Xu L, Yung YC, Santarelli JG, Juan D, Fabel K, Silverberg G, and Harsh G. The temporal–spatial expression of VEGF, angiopoietins-1 and 2, and Tie-2 during tumor angiogenesis and their functional correlation with tumor neovascular architecture. Neurological research 2003; 25:729–38

21. Gevertz JL and Torquato S. Modeling the effects of vasculature evolution on early brain tumor growth. Journal of Theoretical Biology 2006; 243:517–31

22. Martí JM, Garcia-Diaz A, Delgado-Bellido D, O'Valle F, González-Flores A, Carlevaris O, Rodríguez-Vargas JM, Amé JC, Dantzer F, King GL, et al. Selective modulation by PARP-1 of HIF-1α-recruitment to chromatin during hypoxia is required for tumor adaptation to hypoxic conditions. Redox Biology 2021; 41:101885

23. Lobov IB, Brooks PC, and Lang RA. Angiopoietin-2 displays VEGF-dependent modulation of capillary structure and endothelial cell survival in vivo. Proceedings of the National Academy of Sciences 2002; 99:11205–10

24. Holash J, Maisonpierre P, Compton D, Boland P, Alexander C, Zagzag D, Yancopoulos G, and Wiegand S. Vessel cooption, regression, and growth in tumors mediated by angiopoietins and VEGF. Science 1999; 284:1994–8

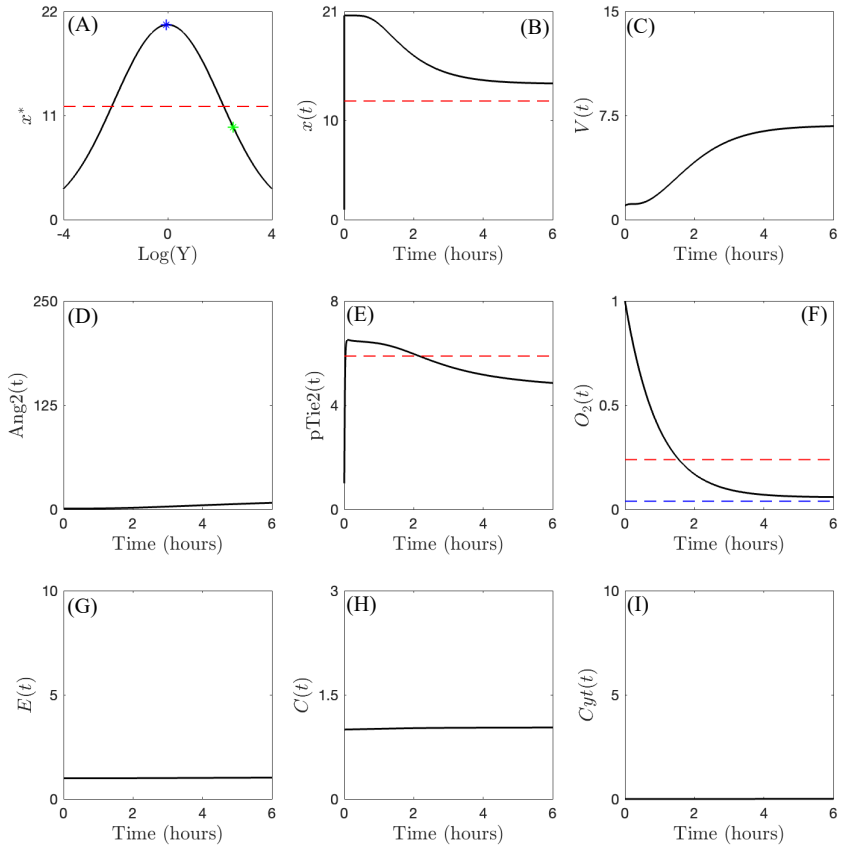

Supplementary Figure 7: **Advanced-stage tumor evolution.** Qualitative results of the evolution of the system (19) for parameter values listed in the Supplementary Table 2 in the advance-stage tumor scenario for $t \in [0, T_0]$ and $T_0 = 0.27$ days. (A) shows the qualitative relationship between Y and the equilibrium state of the dimerized form of VEGFR (x^*), i.e., x^* as a function of $Y := \frac{k_{\text{on}}}{k_{\text{off}}} V$, where k_{on} and k_{off} are the binding and unbinding rates between V and u, respectively [3]. The blue marker indicates the value of x^* for $V(0)$, while the green marker indicates the value of x^* at $V_{\max}$, which represents a numerically observed upper bound for the ligand concentration. Red dashed lines in (A) and (B) refer to the threshold th_x, above which EC proliferation is stimulated, the one in (E) plot to the threshold th_{pTie2}, below which vessel destabilization might happen, the red and blue in (F) refers to normoxia-hypoxia (5% O_2) and hypoxia-severe hypoxia (1% O_2) thresholds, respectively. All the y-axis refer to non-dimensionalized density or concentrations.

25. Kartikasari AE, Huertas CS, Mitchell A, and Plebanski M. Tumor-induced inflammatory cytokines and the emerging diagnostic devices for cancer detection and prognosis. Frontiers in Oncology 2021; 11:692142

26. Zhang T, Xu D, Liu J, Wang M, Duan LJ, Liu M, Meng H, Zhuang Y, Wang H, Wang Y, et al. Prolonged hypoxia alleviates prolyl hydroxylation-mediated suppression of RIPK1 to promote necroptosis and inflammation. Nature cell biology 2023; 25:950–62

27. Casciari JJ, Sotirchos SV, and Sutherland RM. Variations in tumor cell growth rates and metabolism with oxygen concentration, glucose concentration, and extracellular pH. Journal of cellular physiology 1992; 151:386–94

28. McKeown S. Defining normoxia, physoxia and hypoxia in tumours—implications for treatment response. The British journal of radiology 2014; 87:20130676

29. Zheng X, Koh GY, and Jackson T. A continuous model of angiogenesis: initiation, extension, and maturation of new blood vessels modulated by vascular endothelial growth factor, angiopoietins, platelet-derived growth factor-B, and pericytes. Discrete and Continuous Dynamical Systems-Series B 2013; 18:1109–54

30. Maisonpierre PC, Suri C, Jones PF, Bartunkova S, Wiegand SJ, Radziejewski C, Compton D, McClain J, Aldrich TH, Papadopoulos N, et al. Angiopoietin-2, a natural antagonist for Tie2 that disrupts in vivo angiogenesis. Science 1997; 277:55–60

31. Fiedler U, Scharpfenecker M, Koidl S, Hegen A, Grunow V, Schmidt JM, Kriz W, Thurston G, and Augustin HG. The Tie-2 ligand angiopoietin-2 is stored in and rapidly released upon stimulation from endothelial cell Weibel-Palade bodies. Blood 2004; 103:4150–6

32. Alawo DO. Computational modelling of the angiopoietin and tie interactions. PhD thesis. University of Leicester, 2014

33. Alfonso JCL, Köhn-Luque A, Stylianopoulos T, Feuerhake F, Deutsch A, and Hatzikirou H. Why one-size-fits-all vaso-modulatory interventions fail to control glioma invasion: in silico insights. Scientific reports 2016; 6:37283

34. Macklin P, McDougall S, Anderson AR, Chaplain MA, Cristini V, and Lowengrub J. Multiscale modelling and nonlinear simulation of vascular tumour growth. Journal of mathematical biology 2009; 58:765–98

35. Liao KL, Bai XF, and Friedman A. Mathematical modeling of interleukin-27 induction of anti-tumor T cells response. PLoS One 2014; 9:e91844

36. Conte M and Surulescu C. Mathematical modeling of glioma invasion: acid-and vasculature mediated go-or-grow dichotomy and the influence of tissue anisotropy. Applied Mathematics and Computation 2021; 407:126305